Simulation of the magnetoresistance of ultracold atomic Bose gases in bichromatic lattices

J. Towers,[1,2] S. C. Cormack,[1] and D. A. W. Hutchinson[1,2]

[1]*The Jack Dodd Centre for Quantum Technology, Department of Physics, University of Otago, Dunedin, New Zealand*

[2]*Centre for Quantum Technologies, National University of Singapore, 3 Science Drive 2, Singapore 117543*

(Received 20 July 2012; revised manuscript received 14 August 2013; published 18 October 2013)

We present a theoretical study of the two-dimensional ultracold Bose gas in the presence of disorder and bichromatic pseudodisorder in an optical lattice, to which we apply a synthetic magnetic field. We demonstrate that, in the ballistic-transport regime, this leads to positive magnetoresistance and that, in the diffusive and strong-localization regimes, can also lead to negative magnetoresistance. We propose experimental scenarios to observe these effects.

DOI: 10.1103/PhysRevA.88.043625 PACS number(s): 67.85.−d, 05.30.Jp, 71.55.Jv

I. INTRODUCTION

The study of disorder-induced localization in ultracold atomic gases is now well established, with strong localization observed in one-dimensional (1D) quasiperiodic lattices [1] and Anderson localization [2,3] in both one- [4] and three-dimensional (3D) geometries [5,6] with disorder induced through laser speckle [7,8]. In general, localization is always expected in a truly disordered 1D system (although not necessarily in a bichromatic lattice), whereas in 3D there exists a mobility edge [9] between localized and extended states, and a quantum phase transition between metallic and insulating phases can be expected [10]. Two dimensions (2D), as is often the case, is the marginal dimension between these behaviors and, in the solid state, has led to interesting debate [11] regarding the potential observation of a metallic phase in Si MOSFETs. The observation of Anderson localization of ultracold gases in 2D speckle potentials is also complicated [12,13] by the presence of classical trapping in the minima of the speckle potential. Studies of localization in disordered ultracold 2D gases are therefore of timely interest.

Anderson localization is a single-particle interference phenomenon and is strongly enhanced in 2D by the increased occurrence of crossing trajectories (in a path-integral picture) over and above those in 3D. Crossing paths always result in closed loops that constructively interfere back at the origin of the path with their time-reversed equivalent. This enhances the probability that a particle that starts at point **r** remains at point **r**, i.e., is localized. If one introduces a magnetic field (of any orientation in 3D, or with some component perpendicular to the plane in 2D) then this time-reversal symmetry is broken and the enhancement of localization destroyed. This is the origin of *negative magnetoresistance*, which was a 30-year puzzle until explained in the context of Anderson localization [14,15] in 1980. The observation of the analog of such negative magnetoresistance in an ultracold atomic gas localized by disorder would be unambiguous evidence that the localization was an interference phenomenon and not classical trapping or interaction-induced self-trapping. In our understanding, such clarification would be useful in current experiments [12].

Of course, ultracold atoms are charge neutral, so we cannot simply impose an external magnetic field to break the time-reversal symmetry. We can, however, introduce a synthetic magnetic field by rapidly rotating the system [16] or, more practically, through the use of spatially dependent light fields to couple between internal states of the atoms [17–19].

We therefore examine a 2D ultracold Bose gas in an optical lattice with quasiperiodic disorder induced by a weak second lattice of incommensurate wavelength to the first. We then impose a synthetic gauge field based upon the Raman scheme [20] to simulate an applied magnetic field, breaking time-reversal symmetry. We demonstrate that, in the ballistic-transport regime, this leads to magnetoresistance and in the diffusive (weak-localization) and insulating (strong-localization) regimes can induce negative magnetoresistance.

In 1D and in the case of true disorder, all states are localized. However, in the pseudodisorder introduced via a two-color optical lattice as in the Aubry-André model [21], there is a transition from extended states to localized dependent on the strength of the pseudodisorder. This is nicely illustrated by Albert and Leboeuf [22], where they show that above the critical value $\Delta = 2$ of the disorder parameter, in 1D, interference effects lead to the single-particle eigenstates being localized. In some sense this is a classical localization effect, but its origin is still in the interference of the quantum-mechanical single-particle wave functions of the atoms. The localization is therefore still due to an interference phenomenon—just as there are numerous examples [23] of localization of classical waves—although in the pseudodisorder case this may not strictly be Anderson localization. The quantum origin of this interference has also been recently discussed, in the contexts of both correlated speckle disorder and quasiperiodic potentials, by Moratti and Modugno [24]. It is certainly not simply the classical trapping of the gas by the disorder potential itself, which could, in principle, be a concern in 2D speckle experiments, as mentioned above. In the rest of this paper we will therefore not distinguish further and will refer to the localization caused simply as strong localization.

II. THE MODEL

Our system is well described by the Bose-Hubbard Hamiltonian which in the absence of interparticle interactions takes the form

$$\hat{H} = -\sum_{\langle n,m \rangle} J_{n,m} \hat{a}_n^\dagger \hat{a}_m + \sum_n \epsilon_n \hat{a}_n, \tag{1}$$

where $\hat{a}_n$ is the Bose annihilation operator for the nth site, $J_{n,m}$ represents hopping from the nth to the mth site, and $\langle n,m\rangle$ indicates the nearest neighbors m of the nth site [25,26].

Disorder is introduced via interference with a weak optical lattice that is incommensurate with the primary. This, along with an external harmonic trap, is included in the on-site energy term:

$$\epsilon_n = V_{\text{dis}}[\cos(4\pi x_n/\lambda_2 + \phi_x) + \cos(4\pi y_n/\lambda_2 + \phi_y)] + V_{\text{trap}}\left(x_n^2 + y_n^2\right)/\lambda_1^2,$$

where V_{dis} represents the strength of the secondary lattice, V_{trap} the strength of the harmonic confinement, and λ_1 (λ_2) the wavelength of the primary (secondary) lattice.

To include the effect of the synthetic gauge field we first assume that there still exists an orthonormal set of basis states that are localized to each site (modified Wannier functions), then impose gauge invariance for any observable on the Hamiltonian [27–29]. This motivates the modification to the hopping term in (1):

$$J_{n,m} \to J_{n,m}^{(\mathbf{A})} = J_{n,m} \exp\left[-\frac{iq}{\hbar}\int_{\mathbf{x}_n}^{\mathbf{x}_m} \mathbf{A}\cdot d\mathbf{s}\right], \qquad (2)$$

where the integral is taken over the shortest path separating the end points. With this it can be shown that any gauge transformation with a function $f(x,y)$, such that $A \to A' = A + \nabla f$, results in $\hat{a}_n \to \hat{a}'_n = \exp[-iqf/\hbar]\,\hat{a}_n$ and conserves the site number operator ($\hat{n}'_n = |\hat{a}'_n|^2 = |\hat{a}_n|^2 = \hat{n}_n$), therefore satisfying gauge invariance.

The spatial dependence of the hopping terms can be calculated analytically, if one approximates the Wannier functions of the tight-binding model [30] with Gaussians [31–35], or numerically with the (appropriately modified, in the presence of a field) Wannier functions themselves [26]. In the absence of a magnetic field it is our experience [36], and is well established in the literature [31,32], that the spatial dependence of the hopping term is of negligible importance compared to the on-site energy fluctuations. We therefore assume that this remains true in the presence of a magnetic field and set $J_{n,m} = J$.

We then apply the mean-field approximation ($a_n \simeq \langle a_n\rangle = z_n : z_n \in \mathbb{C}$) to the Heisenberg equation of motion for the Bose annihilation operator. It is convenient to relabel the sites according to their spatial position; we therefore define $z_{j,k}$ to be the amplitude of the site located at $(x,y) = (k,j)a_1 : j,k \in \mathbb{Z}$, $a_1 = \lambda_1/2$. The discrete mean-field equations of motion in the Landau gauge ($\mathbf{A} = -By\hat{\mathbf{x}}$) are then given by

$$i\dot{z}_{j,k} = -z_{j-1,k} - z_{j+1,k} - e^{-i\varphi j} z_{j,k-1} - e^{i\varphi j} z_{j,k+1} + \epsilon_{j,k} z_{j,k} \qquad (3)$$

with

$$\epsilon_{j,k} = \Delta[\cos(2\pi\alpha j + \phi_y) + \cos(2\pi\alpha k + \phi_x)] + v_{\text{trap}}(j^2 + k^2), \qquad (4)$$

where the overdot indicates the derivative with respect to scaled time $\tau = t/t_0$, $t_0 = J/\hbar$. $\Delta = V_{\text{dis}}/J$ is the secondary-lattice parameter and $v_{\text{trap}} = V_{\text{trap}}/J$ the harmonic trap parameter. φ is the phase accumulated in the Aharanov-Bohm effect when a charged particle circumnavigates one lattice plaquette in the counterclockwise direction.

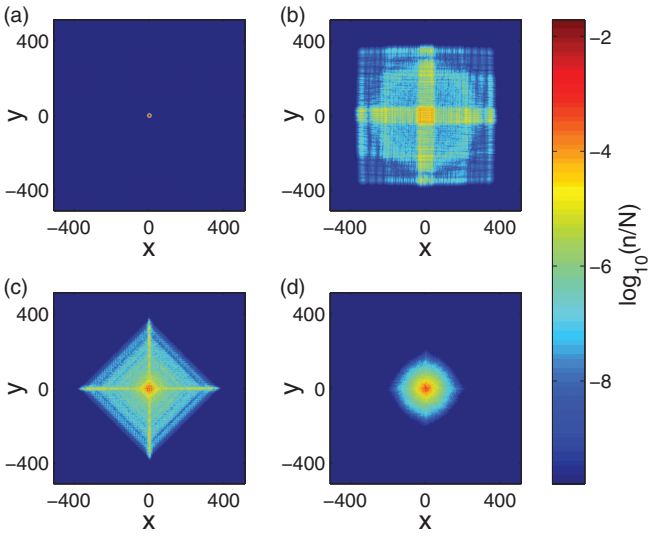

FIG. 1. (Color online) Site occupancy (logarithmic) of (a) the initial wave packet at $t = 0$ and (b)–(d) after propagating for $1000t_0$ (s) in the secondary lattice, with $\Delta = 1$, and synthetic gauge field (b) $\varphi = 0.001$; (c) $\varphi = 0.1$; (d) $\varphi = 1$. Spatial coordinates are in units of site separation (a_1).

If we neglect the synthetic gauge field this system is separable into two 1D systems, each of which, if we set the lattice wavelength ratio α to an irrational number, is equivalent to the Aubry-André model [21]. Therefore, for $\Delta < 2$ the eigenstates are extended and the dynamics is ballistic; for $\Delta = 2$ the dynamics is diffusive; and for $\Delta > 2$ the eigenstates are exponentially localized and we enter the strong-localization regime where, except for virtual transmission on the order of the localization length, conduction is entirely suppressed [37]. In our simulations we use the rational value $\alpha = \frac{1025}{863}$ corresponding to the ratio of wavelengths used in experiments [1]. In the presence of the synthetic gauge field, however, the equations are not separable and we find some interesting dynamics.

For all simulations we initialize the wave packet in the ground state of the primary lattice and a fairly strong harmonic trap ($v_{\text{trap}} = 10^{-2}$). This ground state has radial symmetry in a nearly Gaussian distribution [Fig. 1(a)]. The harmonic trap is then switched off at the same time as the synthetic gauge field and secondary-lattice potential are switched on. The changing magnetic field gives the wave packet a gauge-dependent momentum kick [38]. In the symmetric gauge the wave function remains unchanged as the contributions from the two dimensions cancel. We work in the Landau gauge, however, so we must transform the wave function using $z^L_{j,k} = e^{i\varphi jk/2} z^S_{j,k}$. We then evolve the wave packet in the time domain using a fourth-order Runge-Kutta method [39].

The periodicity of the primary lattice introduces a cosine dispersion relation in the first Brillouin zone. The lowest-momentum states fall on the approximately quadratic part of the dispersion relation and so the motion of an initially low-energy wave packet mimics that of a wave packet in free space but with a reduced effective mass [40]. The motion is termed ballistic as the rms half-width scales as t with time.

In this picture, we can understand our system in the presence of a synthetic gauge field. A classical particle in a magnetic field would complete closed circular loops in the 2D plane. In our simulations, an initially Gaussian distribution expands to a larger Gaussian with a ragged boundary that appears to be rotating. The size to which the Gaussian can expand is determined by the starting size and the size of the classical cyclotron orbits. So far, this system is analogous to that described in [41] which results in the celebrated Hofstadter butterfly, also investigated recently [42] in the context of atomic gases.

III. WEAK PSEUDODISORDER

In the extended regime ($\Delta < 2$), the wave packet released into a negligibly weak magnetic field gains the square symmetry [43] of the reciprocal lattice, with the real-space density at long times reflecting the initial momentum distribution [Fig. 1(b)] and the rms half-width follows the expected t dependence (Fig. 3, triangle) characteristic of ballistic expansion.

When the magnetic field is stronger, time-reversal symmetry is broken and hence the σ_x and σ_y symmetries [44] (reflection in the $x = 0$ and $y = 0$ planes, respectively) are also broken. The $C_2 = \sigma_x\sigma_y$ symmetry (rotation by π) remains, however, and so the solid points and unfilled squares in Fig. 2 are each self-similar and the Bravais lattice and hence the reciprocal lattice are now rotated by $\pi/2$. The lattice parameter is also increased by a factor of $\sqrt{2}$ and hence the "volume" of the Brillouin zone is reduced by half. This results in the diamond symmetry of Fig. 1(c), a signature that would be clearly observable in time-of-flight type experiments. In a very strong gauge field [Fig. 1(d)], the initial momentum distribution no longer fills the entire Brillouin zone and so the expanded wave packet maintains some of the radial symmetry, losing the diamondlike structure.

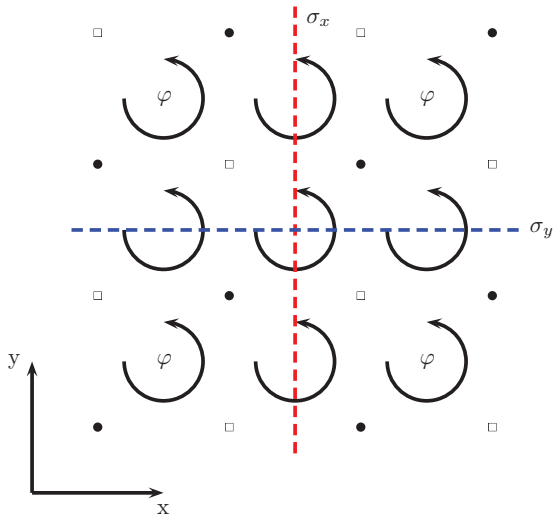

FIG. 2. (Color online) Diagram of the primary lattice depicting the phase accumulated around a lattice plaquette in the synthetic gauge field and the symmetries σ_x and σ_y which are broken. Filled and unfilled dots indicate the loss of self-similarity between these sets of sites due to symmetry breaking.

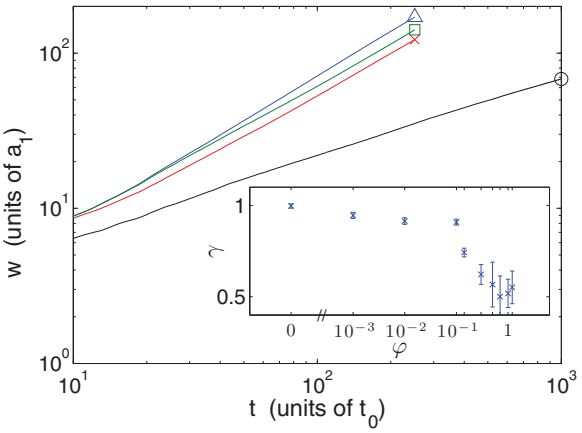

FIG. 3. (Color online) rms half-width of the particle cloud vs time during evolution in a secondary lattice with strength $\Delta = 1$ and synthetic gauge field: (triangle), $\varphi = 0.001$; (square), $\varphi = 0.01$; (cross), $\varphi = 0.1$; (circle), $\varphi = 1$. Inset: Long-term scaling ($w \propto t^{\gamma}$) of the width of the cloud.

At long times, increasing the magnetic field has the effect of decreasing the cloud's rate of expansion (Fig. 3). The classical analogy is that the particles are completing more of their tighter circular orbits, and hence traversing less linear distance, before being scattered off the pseudorandom secondary lattice. This is therefore analogous with normal, positive magnetoresistance.

The durations of the simulations shown in Fig. 4 are limited by the system size; the simulation is terminated when the effect of the periodic boundary conditions becomes noticeable.

In the inset of Fig. 3 we plot $\gamma = \frac{d\log_{10}(w)}{d\log_{10}(t)}$ at long times for a selection of gauge-field strengths. The data points are obtained using a temporal average about each point. The error bars reflect the variance in the data. The long-time behavior of

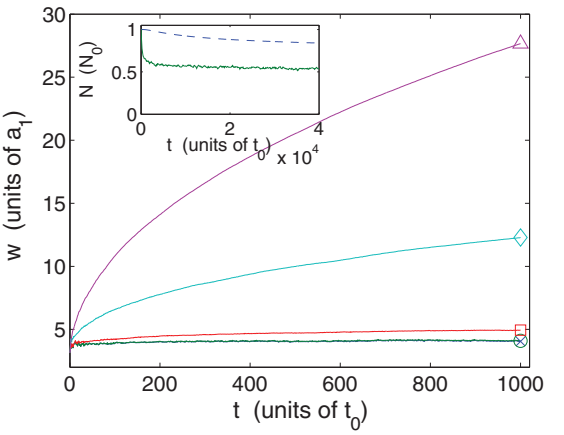

FIG. 4. (Color online) rms half-width of the particle cloud vs time during evolution in a secondary lattice with strength $\Delta = 3$ and synthetic gauge field: (cross), $\varphi = 0.001$; (circle), $\varphi = 0.01$; (square), $\varphi = 0.1$; (diamond), $\varphi = 0.5$; (triangle) $\varphi = 1$. Disorder averaging is performed by sampling a range of pseudoincommensurate lattice ratios about $\alpha = 1.2$. Inset: Total particles vs time when $\Delta = 3$, $\varphi = 1$, and using a 25-site absorbing boundary layer in a (256 × 256)-site system (thus attenuating extended states). (Dashed line), full system; (solid line), 31 × 31 sites at center of the system.

the size of the cloud approaches $t^{1/2}$ with very strong magnetic field, which is characteristic of diffusive expansion.

To summarize, for weak disorder, the effect of the magnetic field is therefore to change the transport from ballistic to diffusive expansion. Furthermore, with increasing field strength, the diffusion coefficient is reduced, consistent with positive magnetoresistance.

IV. STRONG PSEUDODISORDER

In the strongly localized regime, $\Delta > 2$, we observe the confinement of the wave packet consistent with the Aubry-André model for a sufficiently weak gauge field (Fig. 4, square). This localization is the result of the total destructive interference of multiply scattered matter waves for any sites beyond the localization length.

Considering any path that loops back to its origin, the same path traversed in the opposite (time-reversed) direction is of the same length and hence will return the same phase. Any closed path and its time-reversed partner will therefore interfere constructively. In the presence of a gauge field, however, the phase is displaced proportionally to the flux enclosed, which has opposite sign for each direction (the Aharonov-Bohm effect). The two paths will then interfere with an essentially random phase. When averaged over many paths, the backscattering of the matter waves is now dramatically reduced, resulting in the destruction of the localization and a positive expansion of the wave packet.

For a sufficiently strong gauge field we clearly observe the destruction of the strong localization (Fig. 4). Furthermore, increasing the magnetic field increases the rate of expansion of the cloud, characteristic of negative magnetoresistance. The transition occurs continuously, suggesting that the localization is broken for any magnetic-field strength, although it may be undetectable for the system run times that we can simulate.

It is interesting to note that localization is not completely broken for all states. Some of the eigenstates remain localized. In the inset of Fig. 4 we demonstrate the presence of localized eigenstates. For this plot we have included a large negative-imaginary term in the local part of the Hamiltonian for sites within 25 sites of the system edge [in a (256×256)-site system]. When released from the harmonic trap, any outward-bound population is quickly absorbed in the boundary layer before it can create edge effects back at the center. In the plot we observe that the decay of the total population saturates as all the extended states are attenuated when they reach the edge of the simulation grid, leaving behind the surviving localized states. This is most pronounced for the 31×31 sites at the center of the system. Such behavior could be observed experimentally by taking *in situ* absorption images and observing the change in particle number with time.

V. TRUE DISORDER

Up to this point we have considered disorder introduced through a quasiperiodic potential as in the experiments of Roati *et al*. [1] and Schulte *et al*. [45]. We now compare these results to those obtained using a true disorder potential defined by replacing the previous $\epsilon_{j,k}$ with

$$\epsilon_{j,k} = W\mathrm{R} \quad \text{and} \quad (j,k), \tag{5}$$

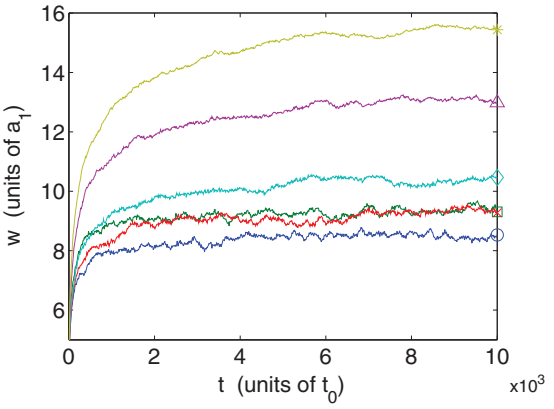

FIG. 5. (Color online) rms half-width of the particle cloud vs time during evolution in a uniformly random on-site potential with energies in the range $[0,9]J$. Synthetic gauge field switched on at $t = 0$ with strength (circle), $\varphi = 0$; (square), $\varphi = 0.001$; (cross), $\varphi = 0.01$; (diamond), $\varphi = 0.1$; (triangle), $\varphi = 0.5$; and (asterisk), $\varphi = 1$.

where W is the strength of the disorder and Rand( ) is MATLAB's random-number generator producing pseudorandom numbers on the interval [0,1] for each lattice site. This model, while strictly unachievable in current experiments, is an approximation to those using 2D laser speckle patterns. However, the disorder potential produced through laser speckle contains correlations due to the grain size which are not included here. This model could, of course, be extended to include these correlations, but is very parameter specific and so neglected here in this more general treatment.

In principle, with true disorder, all states are localized in 2D [15]. The localization length for weak disorder, however, can be very large compared to the system size. We therefore present calculations performed with $W = 9$ (Fig. 5) as this results in a localization length small enough to contain in our numerical simulations. We ran each simulation ten times with different realizations of the disorder potential and present the average of the wave-packet size vs time. In this model, the wave packet remains localized for any phase (φ) of the gauge potential, as one expects from scaling theory. However, the localization length is increased with increasing field strength, consistent with the appearance of negative magnetoresistance in a truly disordered system.

VI. CONCLUSIONS

In conclusion, we have used numerical simulations to demonstrate the interplay between synthetic gauge fields and strong localization in the Aubrey-André model. We observe first positive magnetoresistance in the extended regime and then negative magnetoresistance in the strong-localization regime. We have demonstrated distinctive behaviors for each regime that should be experimentally observable through straightforward absorption imaging techniques. Especially, the observation of negative magnetoresistance can be explained only in the context of an interference phenomenon. This would therefore be an unambiguous signature that localization, destroyed or reduced by the imposition of a magnetic field, had such interference as its origin, distinguishing it from classical trapping or interaction-induced self-trapping. This

is especially important in 2D where ambiguity in the origin of localization in experiments still resides. Whilst our study has concentrated on the use of quasiperiodic lattices for the experimental introduction of the disorder potential, we have demonstrated qualitative agreement for our conclusions using a true disorder potential. We therefore believe our results will carry over to experiments using laser speckle.

ACKNOWLEDGMENTS

We would like to acknowledge financial support from the NZ Foundation for Research, Science and Technology through Contract No. NERF-UOOX0703 and from the National Research Foundation and Ministry of Education of Singapore.

[1] G. Roati, C. D'Errico, L. Fallani, M. Fattori, C. Fort, M. Zaccanti, G. Modugno, M. Modugno, and M. Inguscio, Nature (London) **453**, 895 (2008).
[2] P. W. Anderson, Phys. Rev. **109**, 1492 (1958).
[3] E. Abrahams, *50 Years of Anderson Localization* (World Scientific, Singapore, 2010).
[4] J. Billy *et al*. Nature (London) **453**, 891 (2008).
[5] F. Jendrzejewski *et al*. Nat. Phys. **8**, 398 (2012).
[6] S. S. Kondov, W. R. McGehee, J. J. Zirbel, and B. DeMarco, Science **334**, 66 (2011).
[7] M. Piraud, A. Aspect, and L. Sanchez-Palencia, Phys. Rev. A **85**, 063611 (2012).
[8] L. Sanchez-Palencia and M. Lewenstein, Nat. Phys. **6**, 87 (2010).
[9] M. H. Cohen, H. Fritzsche, and S. R. Ovshinsky, Phys. Rev. Lett. **22**, 1065 (1969).
[10] N. F. Mott, Adv. Phys. **16**, 49 (1967).
[11] S. V. Kravchenko and M. P. Sarachik, Rep. Prog. Phys. **67**, 1 (2004).
[12] Phillipe Bouyer, (private communication); M. Robert-de-Saint-Vincent, J.-P. Brantut, B. Allard, T. Plisson, L. Pezzé, L. Sanchez-Palencia, A. Aspect, T. Bourdel, and P. Bouyer, Phys. Rev. Lett. **104**, 220602 (2010).
[13] L. Pezzé, M. Robert-de-Saint-Vincent, T. Bourdel, J.-P. Brantut, B. Allard, T. Plisson, A. Aspect, P. Bouyer, and L. Sanchez-Palencia, New J. Phys. **13**, 095015 (2011).
[14] P. A. Lee, J. Non-Cryst. Solids **35**, 21 (1980).
[15] P. A. Lee and T. V. Ramakrishnan, Rev. Mod. Phys. **57**, 287 (1985).
[16] K. W. Madison, F. Chevy, W. Wohlleben, and J. Dalibard, Phys. Rev. Lett. **84**, 806 (2000).
[17] J. Dalibard *et al*., Rev. Mod. Phys. **83**, 1523 (2011).
[18] D. Jaksch and P. Zoller, New J. Phys. **5**, 56 (2003).
[19] E. J. Mueller, Phys. Rev. A **70**, 041603 (2004).
[20] Y.-J. Lin, R. L. Compton, K. Jiménez-Garcia, J. V. Porto, and I. B. Spielman, Nature (London) **462**, 628 (2009).
[21] S. Aubry and G. André, Ann. Isr. Phys. Soc. **3**, 133 (1980).
[22] M. Albert and P. Leboeuf, Phys. Rev. A **81**, 013614 (2010).
[23] D. R. Luhman, J. C. Herrmann, and R. B. Hallock, Phys. Rev. Lett. **94**, 176401 (2005).
[24] M. Moratti and M. Modugno, Eur. Phys. J. D **66**, 138 (2012).
[25] G. H. Wannier, Rev. Mod. Phys. **34**, 645 (1962).
[26] O. Morsch and M. Oberthaler, Rev. Mod. Phys. **78**, 179 (2006).
[27] T. B. Boykin, R. C. Bowen, and G. Klimeck, Phys. Rev. B **63**, 245314 (2001).
[28] M. Graf and P. Vogl, Phys. Rev. B **51**, 4940 (1995).
[29] J. M. Luttinger, Phys. Rev. **84**, 814 (1951).
[30] D. W. Bullett, Solid State Phys. **35**, 129 (1980).
[31] F. Schmitt, M. Hild, and R. Roth, Phys. Rev. A **80**, 023621 (2009).
[32] V. Guarrera, L. Fallani, J. E. Lye, C. Fortand, and M. Inguscio, New J. Phys. I **9**, 107 (2007).
[33] T. Roscilde, Phys. Rev. A **77**, 063605 (2008).
[34] M. Modugno and G. Pettini, New J. Phys. **14**, 055004 (2012).
[35] W. Zwerger, J. Opt. B **5**, S9 (2003).
[36] C. P. J. Adolphs *et al*., arXiv:1101.5406v1.
[37] M. Larcher, F. Dalfovo, and M. Modugno, Phys. Rev. A **80**, 053606 (2009).
[38] Y-J. Lin, R. L. Compton, K. Jimnez-Garca, W. D. Phillips, J. V. Porto, and I. B. Spielman, Nat. Phys. **7**, 531 (2011).
[39] William H. Press, Saul A. Teukolsky, William T. Vetterling, and Brian P. Flannery, *Numerical Recipes*, 3rd ed. (Cambridge University Press, Cambridge, 2007).
[40] N. W. Ashcroft and N. D. Mermin, *Solid State Physics* (Harcourt Brace College, Forth Worth, 1976).
[41] D. R. Hofstadter, Phys. Rev. B **14**, 2239 (1976).
[42] S. Powell, R. Barnett, R. Sensarma, and S. DasSarma, Phys. Rev. A **83**, 013612 (2011).
[43] U. Schneider, L. Hackermüller, J. P. Ronzheimer, S. Will, S. Braun, T. Best, I. Bloch, E. Demler, S. Mandt, D. Rasch, and A. Rosch, Nat. Phys. **8**, 213 (2012).
[44] S. J. Joshua, *Symmetry Principles and Magnetic Symmetry in Solid State Physics* (Adam Hilger, Bristol, 1991).
[45] T. Schulte, S. Drenkelforth, J. Kruse, W. Ertmer, J. Arlt, K. Sacha, J. Zakrzewski, and M. Lewenstein, Phys. Rev. Lett. **95**, 170411 (2005).